Comp. Meth. Civil Eng., Vol. 2 No. 1 (2011) pp. 65-81

CMCE
Computational Methods in Civil Engineering

Three dimensional static and dynamic analysis of thick plates by the meshless local Petrov-Galerkin (MLPG) method under different loading conditions

A. Rezaei Mojdehi[a,*], A. Darvizeh[a,b], A. Basti [a]

[a] *Department of Mechanical engineering, Faculty of Engineering, University of Guilan, Rasht, Iran*
[b] *Department of Mechanical Engineering, Faculty of Engineering, Islamic Azad University, Anzali Branch, Bandar-e-Anzali, Iran*

Received 6 April 2011; accepted 12 May 2011

Abstract

In this paper, three dimensional (3D) static and dynamic analysis of thick plates based on the Meshless Local Petrov-Galerkin (MLPG) is presented. Using the kinematics of a three-dimensional continuum, the local weak form of the equilibrium equations is derived. A weak formulation for the set of governing equations is transformed into local integral equations on local sub-domains by using a unit test function. Nodal points are distributed in the 3D analysis domain and each node is surrounded by a cubic sub-domain to which a local integral equation is applied. The meshless approximation based on the three dimensional Moving Least-Square (MLS) is employed as the shape function to approximate the field variable of scattered nodes in the problem domain. The Newmark time integration method is used to solve the system of coupled second order ODEs. The essential boundary conditions are enforced by the direct interpolation method. Numerical examples for solving the static and transient response of elastic thick plates are demonstrated. The numerical efficiency of the proposed meshless method is demonstrated by comparing the results obtained with the available analytical and/or numerical solutions in the literature.

Keywords: Meshless local Petrov-Galerkin method; Static analysis; Dynamic analysis; Three dimensional moving least square approximation; Thick plates.

1. Introduction

Plates and plate-type structures have gained special importance and notably increased applications in recent years. A large number of structural components in engineering structures and aerospace, civil and ship engineering can be classified as plates. They may be homogeneous, laminated or functionally graded and their thickness depends upon the applications. In this regards, static and dynamic response of plates is very important in

*Corresponding author.
E-mail addresses: a.r.mojdehi@gmail.com (A. Rezaei Mojdehi)

computational mechanics. Exact analyses of these types of boundary and initial value problems are usually very complicated. Analytical solutions are available for very few problems with very simple geometry and boundary and initial conditions. Therefore, numerical techniques with different discretization schemes, such as FEM, have been widely used in solving practical static and dynamic problems in science and engineering.

During recent years, meshless approaches have attracted considerable attention due to their capability to solve a boundary value problem without a meshing procedure. In contrast to the finite element formulation, computational model is described only by a set of nodes which don't need to be connected into elements. Thus, the nodes can be easily added and removed without burdensome remeshing of the entire structure. Furthermore, by using the meshless formulation many other difficulties associated with the finite element method may also be overcome. A variety of these methods have been developed which include element-free Galerkin method [1], the reproducing kernal particle method [2], hp-clouds [3], the partition of unity method [4], meshless Galerkin using radial basis functions [5], the diffuse element [6], the natural element [7], the smoothed particle hydrodynamics [8], the collocation technique employing radial basis functions [9] and the modified smoothed particle hydrodynamics [10]. Of these, the last three methods do not require any mesh whereas others generally need a background mesh for the evaluation of integrals appearing in the weak formulation of the problem. But, the other methods use a background mesh to numerically evaluate integrals appearing in the global weak formulation of the problem.

The meshless local Petrov–Galerkin (MLPG) method developed by Atluri and his colleagues [11–14] is based on local weak rather than the global weak formulation of the problem, and does not require a background mesh for the evaluation of integrals in the weak formulation of the problem. The MLPG methods have been employed in a wide range of applications, for example elasto-statics [15], elasto- dynamics [16], fluid mechanics [17], convection–diffusion problems [18], thermoelasticity [19], beam problems [20-21], fracture mechanics [22-23] and strain gradient theory [24].

MLPG method has been used to analyze deformations of plate-type structures. Gu and Liu [25] used the MLPG method to study static and free vibration analyses of thin plates. Long and Atluri [26] utilized MLPG method for solving the bending problem of a thin plate. Qian et al. [27] developed two MLPG methods for elastostatic deformations of a thick plate by using a Higher-Order Shear and Normal Deformable Plate Theory (HOSNDPT). Soric et al. [28] used separate interpolation in thickness direction for analysis of thick plates. Li et al. [29] developed a locking-free MLPG formulation for thick and thin plates. Xiao et al. [30] combined MLPG method with the Higher-Order Shear and Normal Deformable Plate Theory (HOSNDPT) with radial basis functions to analysis of plates. Sladek et al. [31] used MLPG method for Reissner–Mindlin plates under dynamic load.

After many pioneering research studies were successfully carried out for 2D problems, the MLPG methods are becoming more attractive for solving 3D problems, because of their distinct advantages over the element-based methods. The representative 3D works include the papers [32-35] for 3D elastic problems by using MLPG domain methods. It has been reported that the MLPG methods give better accuracy with lesser CPU time and lesser system resources, than the element-based methods [14,33,36]. It makes the MLPG method to be more efficient, in solving large-scale dynamic problems.

In this paper, 3D static and dynamic analysis of thick plates based on the MLPG approaches is presented. Galerkin weak-form formulation is applied to derive the discrete governing equilibrium equations in a three dimensional continuum. A weak formulation for the set of governing equations is transformed into local integral equations on local sub-domains by using a unit test function. The meshless approximation based on the three dimensional Moving Least-Square (MLS) is employed as shape function to approximate the

field variable of scattered nodes in the problem domain. The Newmark time integration method is used to solve the system of coupled second order Ordinary Differential Equations (ODEs). The essential boundary conditions are enforced by the direct interpolation method. As results, the influence of the size of the weight function support on the plate central deflection is investigated and the convergence rate of the central deflection of the plate for different nodal distributions is introduced. The numerical efficiency of the proposed meshless method is demonstrated by comparing the results obtained with the available analytical and/or numerical solutions in the literature.

2. MLPG formulation for 3D solids

According to a three dimensional solid concept, the equilibrium equations in a domain of the volume Ω, which is bounded by the surface Γ, are given by:

$$\sigma_{ij,j} + b_i = \rho\ddot{u}_i, \qquad \text{in } \Omega \tag{1}$$

where σ_{ij} are the components of the symmetric stress tensor, b_i are the body forces, the indices i, j which take the values 1, 2 and 3 refer to the coordinates x, y, z on the boundary Γ. The following boundary conditions are assumed:

$$u_i = \bar{u}_i, \qquad on\ \Gamma_u \tag{2a}$$

$$t_i = \sigma_{ij} n_j = \bar{t}_i, \qquad on\ \Gamma_t \tag{2b}$$

where $\bar{u}_i$ are the prescribed displacements, $\bar{t}_i$ are the prescribed surface tractions, n_j are the components of a unit outward normal to the global boundary, Γ_u is the part of global boundary with prescribed displacements, and Γ_t is the part of global boundary with prescribed surface tractions.

Initial conditions for dynamic analysis are:

$$u_i(\mathbf{x}, t)|_{t=0} = \tilde{u}_i(\mathbf{x}, 0) \quad \mathbf{x} \in \Omega \tag{3a}$$

$$\dot{u}_i(\mathbf{x}, t)|_{t=0} = \tilde{\dot{u}}_i(\mathbf{x}, 0) \quad \mathbf{x} \in \Omega \tag{3b}$$

where $\tilde{u}_i(\mathbf{x})$ and $\tilde{\dot{u}}_i(\mathbf{x})$ are the values of the initial displacements and velocities, respectively.

Based on the local Petrov-Galerkin approaches, a generalized local weak form of the equilibrium equation over a local sub-domain Ω_q, can be written as:

$$\int_{\Omega q} (\sigma_{ij,j} + b_i - \rho\ddot{u}_i) v_i \, d\Omega = 0 \tag{4}$$

Herein u_i is the trial function describing the displacement field, while v_i is the test function. In the MLPG method applied, the test and trial functions may be chosen from different functional spaces.

By applying the divergence theorem, equation (4) may be rewritten in as:

$$\sigma_{ij,j} v_i = (\sigma_{ij} v_i)_{,j} - \sigma_{ij} v_{i,j} \tag{5}$$

$$\int_{\Gamma_q} \sigma_{ij} n_j v_i \, d\Gamma - \int_{\Omega_q} (\sigma_{ij} v_{i,j} + \rho\ddot{u}_i v_i - b_i v_i) d\Omega = 0 \tag{6}$$

By imposing the natural boundary conditions in equation (2b) one obtains:

$$\int_{\Gamma_{qi}} t_i v_i \, d\Gamma + \int_{\Gamma_{qu}} t_i v_i \, d\Gamma + \int_{\Gamma_{qt}} \bar{t}_i v_i \, d\Gamma - \int_{\Omega_q} \left(\sigma_{ij} v_{i,j} + \rho \ddot{u}_i v_i - b_i v_i\right) d\Omega = 0 \qquad (7)$$

where Ω_q has composed by three parts, i.e. $\Gamma_q = \Gamma_{qi} \cup \Gamma_{qu} \cup \Gamma_{qt}$, in which Γ_{qi} is the internal boundary of the local sub-domain, which does not intersect with the global boundary Γ; Γ_{qt} is the part of the natural boundary that intersects with the local sub-domain and Γ_{qu} is the part of the essential boundary that intersects with the local sub-domain. Figure 1, shows the local sub-domain used in the MLPG method.

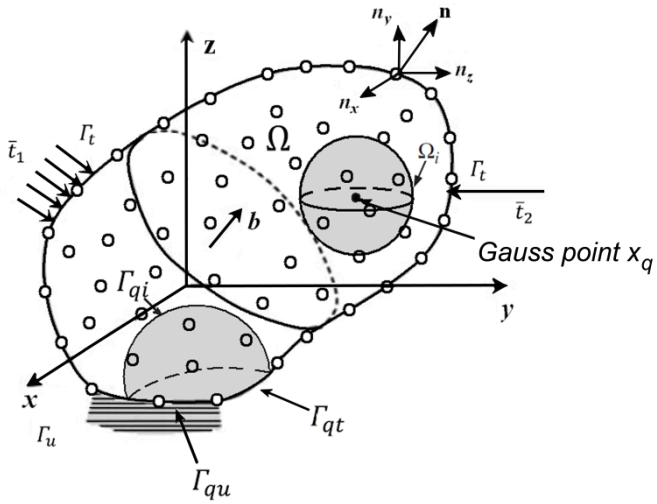

Figure 1. Local domains used in the MLPG method.

Equation (7) may be rewritten as:

$$\int_{\Omega_q} \left(\sigma_{ij} v_{i,j} + \rho \ddot{u}_i v_i\right) d\Omega - \int_{\Gamma_{qi}} t_i v_i \, d\Gamma - \int_{\Gamma_{qu}} t_i v_i \, d\Gamma = \int_{\Gamma_{qt}} \bar{t}_i v_i \, d\Gamma + \int_{\Omega_q} b_i v_i \, d\Omega \qquad (8)$$

which represents a set of three equations for each local sub-domain. The test function v_i is chosen such that it is positive inside the local sub-domain Ω_q and vanishes outside of Ω_q.

3. Numerical discretization

The plate continuum is discretized by the nodes located on the problem domain. The nodal variables are three fictitious displacement components in the Cartesian coordinate system *x, y, z*. The axes *x* and *y* lie in the middle surface, while *z* is directed over the thickness. Using the MLS shape functions, we can approximate the trial function for the displacement at each point. The MLS approximation of $u(\mathbf{x})$ is defined at x as:

$$u^h(\mathbf{x}) = \sum_{i=1}^{m} p_i(\mathbf{x}) a_i(\mathbf{x}) = \mathbf{p}^{\mathrm{T}}(\mathbf{x}) \mathbf{a}(\mathbf{x}) \quad \forall \mathbf{x} \in \Omega \qquad (9)$$

where $\mathbf{p}^T(\mathbf{x}) = [p_1(\mathbf{x}), p_2(\mathbf{x}), \ldots, p_m(\mathbf{x})]$ is a vector of complete basis functions of order *m* and $\mathbf{a}(\mathbf{x})$is a vector containing the coefficients $a_i(\mathbf{x}), i = 1, 2, \ldots, m$, which are functions of the space coordinates $\mathbf{x} = [x, y, z]^{\mathrm{T}}$. In 3D problems, the linear basis is defined as:

$$\mathbf{p}^{\mathrm{T}}(\mathbf{x}) = [1, x, y, z];\ m = 4 \tag{10}$$

and the quadratic basis is defined as:

$$\mathbf{p}^{\mathrm{T}}(\mathbf{x}) = [1, x, y, z, x^2, y^2, z^2, xy, yz, xz];\ m = 10 \tag{11}$$

The coefficient vector function $a_i(\mathbf{x})$ is determined by minimizing a weighted discrete L_2 norm, which is defined as:

$$J(\mathbf{x}) = \sum_{I=1}^{N} \mathrm{w}_I(\mathbf{x})[\mathbf{p}^{\mathrm{T}}(\mathbf{x}_I)\mathbf{a}(\mathbf{x}) - \hat{u}^I]^2 \tag{12}$$

where $\hat{u}^I$ are the fictitious nodal values and w_I is the weight function associated with the node I. N is the number of nodes in the support domain for which the weight function $\mathrm{w}_I(\mathbf{x}) > 0$. The Gaussian weight function with compact supports is considered in the present work. The Gaussian weight function corresponding to node I may be written as:

$$\mathrm{w}_I(\mathbf{x}) = \begin{cases} \dfrac{\exp[-(d_I/c_I)^{2k}] - \exp[-(r_I/c_I)^{2k}]}{1 - \exp[-(r_I/c_I)^{2k}]} & 0 \le d_I \le r_I \\ 0 & d_I > r_I \end{cases} \tag{13}$$

where $d_I = \|\mathbf{x} - \mathbf{x}_I\|$ is the distance from node $\mathbf{x}_I$ to point $\mathbf{x}$; c_I is a constant controlling the shape of the weight function w_I and determines the support of node $\mathbf{x}_I$. In the present computation, $k=1$ and $c_I=l_I$ was chosen, where l_I is defined as the Ith smallest distance between node I and the other nodes. Even though the definition of all constant c_I is more or less arbitrary, they do affect the computational results significantly [13]. r_I is the size of weight function support in which the weight function w_I associated with node $\mathbf{x}_I$ is non-zero.
The stationary condition of J in equation (11) with respect to $\mathbf{a}(\mathbf{x})$,

$$\partial J/\partial \mathbf{a} = 0 \tag{14}$$

leads to the following linear relation between fictitious ($\hat{u}$) and approximated (u^h) nodal displacements:

$$u^h(\mathbf{x}) = \sum_{I=1}^{N} \Phi^I(\mathbf{x})\hat{u}^I = \mathbf{\Phi}^{\mathrm{T}}(\mathbf{x})\hat{\mathbf{u}} \tag{15}$$

where $\mathbf{\Phi}^{\mathrm{T}}(\mathbf{x})$ can then be described as the shape function associated with the nodes and is given as:

$$\mathbf{\Phi}^{T}(\mathbf{x}) = \mathbf{P}^{\mathrm{T}}(\mathbf{x})\mathbf{A}^{-1}(\mathbf{x})\mathbf{B}(\mathbf{x}) \tag{16}$$

where,

$$\mathbf{A}(\mathbf{x}) = \sum_{I=1}^{N} \mathrm{w}_I(\mathbf{x})\, \mathbf{p}(\mathbf{x}_I)\mathbf{p}^{\mathrm{T}}(\mathbf{x}_I) = \mathbf{P^T W P} \tag{17}$$

$$\mathbf{B}(\mathbf{x}) = [\mathrm{w}_1(\mathbf{x})\mathbf{p}(\mathbf{x}_1), \mathrm{w}_2(\mathbf{x})\mathbf{p}(\mathbf{x}_2), \dots, \mathrm{w}_N(\mathbf{x})\mathbf{p}(\mathbf{x}_{\mathrm{N}})] = \mathbf{P^T W} \tag{18}$$

where,

$$\mathbf{P} = \begin{bmatrix} \mathbf{p}^{\mathrm{T}}(\mathbf{x}_1) \\ \mathbf{p}^{\mathrm{T}}(\mathbf{x}_2) \\ \vdots \\ \mathbf{p}^{\mathrm{T}}(\mathbf{x}_{\mathrm{N}}) \end{bmatrix}_{N\times m} \tag{19}$$

and,

$$\mathbf{W} = \begin{pmatrix} \mathrm{w}_1(\mathbf{x}) & \cdots & 0 \\ \vdots & \ddots & \vdots \\ 0 & \cdots & \mathrm{w}_N(\mathbf{x}) \end{pmatrix}_{N\times N} \tag{20}$$

The stress tensor components σ_{ij} may be written in a Cartesian coordinate system as a column matrix σ:

$$\boldsymbol{\sigma}^{\mathrm{T}} = \begin{bmatrix} \sigma_x & \sigma_y & \sigma_z & \tau_{xy} & \tau_{yz} & \tau_{zx} \end{bmatrix} \tag{21}$$

Using the generalized Hooke's law, the stress tensor components may be expressed in terms of the nodal unknown variables by the relation:

$$\boldsymbol{\sigma} = \sum_{\mathrm{j}=1}^{\mathrm{N}} \mathbf{D}\mathbf{B}_{\mathrm{j}}\mathbf{u}_{\mathrm{j}} \tag{22}$$

where $\mathbf{D}$ is the three-dimensional stress-strain matrix and $\mathbf{B}_{\mathrm{j}}$ denotes the strain-displacement matrix obtained by differentiation of the shape function in a three dimensional space:

$$\mathbf{D} = D_0 \begin{bmatrix} 1 & \frac{\nu}{1-\nu} & \frac{\nu}{1-\nu} & 0 & 0 & 0 \\ \frac{\nu}{1-\nu} & 1 & \frac{\nu}{1-\nu} & 0 & 0 & 0 \\ \frac{\nu}{1-\nu} & \frac{\nu}{1-\nu} & 1 & 0 & 0 & 0 \\ 0 & 0 & 0 & \frac{1-2\nu}{2(1-\nu)} & 0 & 0 \\ 0 & 0 & 0 & 0 & \frac{1-2\nu}{2(1-\nu)} & 0 \\ 0 & 0 & 0 & 0 & 0 & \frac{1-2\nu}{2(1-\nu)} \end{bmatrix} \tag{23}$$

$$D_0 = \frac{E(1-\nu)}{(1+\nu)(1-2\nu)} \tag{24}$$

$$\mathbf{B}_{(6\times 3N)} = \begin{bmatrix} \frac{\partial \Phi_1}{\partial x} & 0 & 0 & \dots & \frac{\partial \Phi_N}{\partial x} & 0 & 0 \\ 0 & \frac{\partial \Phi_1}{\partial y} & 0 & \dots & 0 & \frac{\partial \Phi_N}{\partial y} & 0 \\ 0 & 0 & \frac{\partial \Phi_1}{\partial z} & \dots & 0 & 0 & \frac{\partial \Phi_N}{\partial z} \\ \frac{\partial \Phi_1}{\partial y} & \frac{\partial \Phi_1}{\partial x} & 0 & \dots & \frac{\partial \Phi_N}{\partial y} & \frac{\partial \Phi_N}{\partial x} & 0 \\ 0 & \frac{\partial \Phi_1}{\partial z} & \frac{\partial \Phi_1}{\partial y} & \dots & 0 & \frac{\partial \Phi_N}{\partial z} & \frac{\partial \Phi_N}{\partial y} \\ \frac{\partial \Phi_1}{\partial z} & 0 & \frac{\partial \Phi_1}{\partial x} & \dots & \frac{\partial \Phi_N}{\partial z} & 0 & \frac{\partial \Phi_N}{\partial x} \end{bmatrix} \tag{25}$$

The surface traction components t_i may also be expressed in a vector form by the relation:

$$\mathbf{t} = \mathbf{N}\boldsymbol{\sigma} = \sum_{j=1}^{N} \mathbf{N}\mathbf{D}\mathbf{B}_j \mathbf{u}_j \tag{26}$$

which **N** is the matrix describing the outward normal on Γ_q,

$$\mathbf{N} = \begin{bmatrix} n_x & 0 & 0 & n_y & 0 & n_z \\ 0 & n_y & 0 & n_x & n_z & 0 \\ 0 & 0 & n_z & 0 & n_y & n_x \end{bmatrix} \tag{27}$$

By means of equations (15), (22) and (26), equation (6) is transformed in the discretized system of ordinary differential equations which may be written in the matrix form:

$$\mathbf{M}\ddot{\mathbf{u}} + \mathbf{K}\mathbf{u} = \mathbf{F} \tag{28}$$

where **M**, **K** and **F** are equivalent mass, stiffness and force matrix, respectively which are described in the following:

$$M_{ij} = \int_{\Omega_q} \rho \Phi_i v_i d\Omega \tag{29}$$

$$K_{ij} = \int_{\Omega_q} \left(\widehat{\mathbf{W}}_i^{\,T} \mathbf{D}\mathbf{B}_j \right) d\Omega - \int_{\Gamma_{qi}} v_i \mathbf{N}\mathbf{D}\mathbf{B}_j \, d\Gamma - \int_{\Gamma_{qu}} v_i \mathbf{N}\mathbf{D}\mathbf{B}_j \, d\Gamma \tag{30}$$

$$F_{ij} = \int_{\Gamma_{qt}} \bar{t}_i v_i \, d\Gamma + \int_{\Omega_q} b_i v_i \, d\Omega \tag{31}$$

By using weight function as test function we have:

$$v_I = \begin{bmatrix} w(\mathbf{x}, \mathbf{x}_I) & 0 & 0 \\ 0 & w(\mathbf{x}, \mathbf{x}_I) & 0 \\ 0 & 0 & w(\mathbf{x}, \mathbf{x}_I) \end{bmatrix} \tag{32}$$

$$\widehat{\mathbf{W}}_I = \begin{bmatrix} w_{,x} & 0 & 0 & w_{,y} & 0 & w_{,z} \\ 0 & w_{,y} & 0 & w_{,x} & w_{,z} & 0 \\ 0 & 0 & w_{,z} & 0 & w_{,y} & w_{,x} \end{bmatrix} \tag{33}$$

Equations similar to equation (28) with mass, stiffness and force matrix as equations (29-31) are obtained for each cubic local sub-domain Ω_q whose centre is at the node xi. The Gauss quadrature rule of an appropriate order is employed to evaluate integrals over each local sub-domain.

4. Time integration

The Newmark β method [37], well known and commonly applied in computations, is used in the present study to integrate the governing equations in time. The recursive relation among displacements, velocities at times *t* and $t + \Delta t$ are:

$$u^{t+\Delta t} = u^t + \Delta t \dot{u}^t + \frac{\Delta t^2}{2}[(1-2\beta)\ddot{u}^t + 2\beta\ddot{u}^{t+\Delta t}] \tag{34}$$

$$\dot{u}^{t+\Delta t} = \dot{u}^t + \Delta t[(1-\gamma)\ddot{u}^t + \gamma\ddot{u}^{t+\Delta t}] \tag{35}$$

where β and γ are constant, for zero damping system, this method is unconditionally stable if:

$$2\beta \geq \gamma \geq \frac{1}{2} \tag{36}$$

and conditionally stable if:

$$\gamma \geq \frac{1}{2} \ , \beta \geq \frac{1}{2} \tag{37}$$

$$\Delta t \leq \frac{1}{\omega_{max}\sqrt{\frac{\gamma}{2} - \beta}} \tag{38}$$

where ω_{max} is the maximum frequency in the structural system.

By setting $\beta = 1/4 \ , \gamma = 1/2$ it results in the constant acceleration scheme. It is non-dissipative, second-order accurate and unconditionally stable. Writing equation (28) at time $t + \Delta t$, and substituting from equations (34) and (35) give the following system of algebraic equations:

$$\hat{\mathbf{K}}^{t+\Delta t}\mathbf{u}^{t+\Delta t} = \hat{\mathbf{F}}^{t+\Delta t} \tag{39}$$

where,

$$\hat{\mathbf{K}}^{t+\Delta t} = \mathbf{K}^{t+\Delta t} + \frac{4}{\Delta t^2}\mathbf{M}^{t+\Delta t} \tag{40}$$

and,

$$\hat{\mathbf{F}}^{t+\Delta t} = \mathbf{F}^{t+\Delta t} + \mathbf{M}^{t+\Delta t}\left(\frac{4}{\Delta t^2}u^t + \frac{4}{\Delta t}\dot{u}^t + \ddot{u}^t\right) \tag{41}$$

having computed $u^{t+\Delta t}$ from equation (39), $\dot{u}^{t+\Delta t}$ and $\ddot{u}^{t+\Delta t}$ are obtained from:

$$\ddot{u}^{t+\Delta t} = \frac{4}{\Delta t^2}(u^{t+\Delta t} - u^t) - \frac{4}{\Delta t}\dot{u}^t - \ddot{u}^t \tag{42}$$

$$\dot{u}^{t+\Delta t} = \dot{u}^t + \frac{\Delta t}{2}(\ddot{u}^t + \ddot{u}^{t+\Delta t}) \tag{43}$$

5. Enforcement of essential boundary conditions

To enforce essential boundary conditions, the direct interpolation method is used [38]. Note that, in MLPG, the system equation is constructed node by node. There are only three rows in the global stiffness matrix and the global force vector that are related to each field node in the 3D formulation. With this structural feature of the system equation of MLPG, the following procedure can be implemented.

Assume the displacements at the *I*th field node on the boundary where the essential boundary are prescribed as:

$$\begin{cases} (u_x^h)^I = \bar{u}_x^I \\ \left(u_y^h\right)^I = \bar{u}_y^I \\ (u_z^h)^I = \bar{u}_z^I \end{cases} \tag{44}$$

where u_x^h , u_y^h and u_z^h are approximated displacements in *x*, *y* and *z* direction, respectively. Using the MLS approximation, one has,

$$\begin{aligned} (u^h)^I = \begin{pmatrix} (u_x^h)^I \\ \left(u_y^h\right)^I \\ (u_z^h)^I \end{pmatrix} &= \begin{pmatrix} \Phi_1 & 0 & 0 & \dots & \Phi_n & 0 & 0 \\ 0 & \Phi_1 & 0 & \dots & 0 & \Phi_n & 0 \\ 0 & 0 & \Phi_1 & \dots & 0 & 0 & \Phi_n \end{pmatrix} \begin{pmatrix} \hat{u}_x^1 \\ \hat{u}_y^1 \\ \hat{u}_z^1 \\ \vdots \\ \hat{u}_x^n \\ \hat{u}_y^n \\ \hat{u}_z^n \end{pmatrix} = \boldsymbol{\Phi}\hat{\mathbf{u}} \\ &= \begin{pmatrix} \bar{u}_x^I \\ \bar{u}_y^I \\ \bar{u}_z^I \end{pmatrix} \end{aligned} \tag{45}$$

where *n* is number of nodes in the support domain of the *I*th node. equation (45) produces three linear equations for the *I*th field node, and can be rewritten explicitly as:

$$\begin{cases} \Phi_1\hat{u}_x^1 + \Phi_2\hat{u}_x^2 + \cdots + \Phi_n\hat{u}_x^n = \bar{u}_x^I \\ \Phi_1\hat{u}_y^1 + \Phi_2\hat{u}_y^2 + \cdots + \Phi_n\hat{u}_y^n = \bar{u}_y^I \\ \Phi_1\hat{u}_z^1 + \Phi_2\hat{u}_z^2 + \cdots + \Phi_n\hat{u}_z^n = \bar{u}_z^I \end{cases} \tag{46}$$

Equation (46) is assembled directly into the system equations for the field nodes to obtain the modified global system equations of,

$$\widehat{\mathbf{K}}_{\mathrm{c}}^{\mathrm{t}+\Delta\mathrm{t}}\mathbf{u}^{\mathrm{t}+\Delta\mathrm{t}} = \widehat{\mathbf{F}}_{\mathrm{c}}^{\mathrm{t}+\Delta\mathrm{t}} \tag{47}$$

where $\widehat{\mathbf{K}}_{\mathrm{c}}^{\mathrm{t}+\Delta\mathrm{t}}$ and $\widehat{\mathbf{F}}_{\mathrm{c}}^{\mathrm{t}+\Delta\mathrm{t}}$ are modified global stiffness matrix and force vector, respectively.

6. Results and Discussion

Numerical results are presented for plates under static and dynamic loading. To test the convergence and the accuracy of the present method, the influence of the size of the weight function, order of basis function and number of nodes in thickness direction for different nodal distributions are investigated. In dynamic loading, by using obtained value of weight function support size from static loading, a clamped and a cantilever square plate subjected to different loading conditions are analyzed.

6.1. Static load

A clamped square plate subjected to the uniformly distributed load over the upper surface is considered. Figure 2 shows the geometry, boundary conditions and loading surface of the plate. The plate thickness to span ratio is $h/a = 0.1$. The material data are Young's modulus E=1 MPa and Poisson's ratio $\nu = 0.3$. Due to symmetry, only one quarter of the plate is discretized by the various uniformly distributed nodal points on the domain of the plate. The discretization by $9 \times 9 \times 3$ nodes is shown in Figure 3.

The influence of the size of the weight function support on the plate central deflection is investigated. It is found that the weight function support significantly affects the numerical solutions. Dependency of the plate central deflection on the ratio of the support radius to the radius of local sub-domain for different number of nodal points with quadratic basis is plotted in Figure 4.

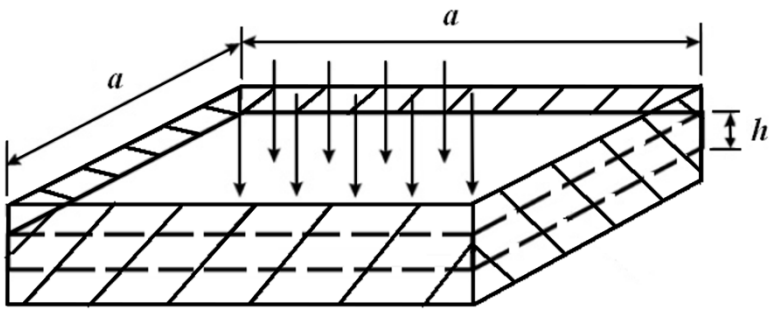

Figure 2. Clamped square plate subjected to uniform load.

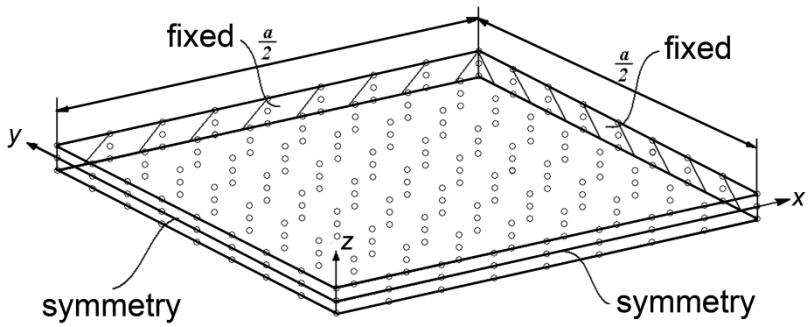

Figure 3. Discretization of one quarter of the square plate.

In the present analysis, cubic support domain is used as weight function domain of influence and also local sub-domain is used for quadrature domain. For a cubic support domain, the dimensions of the support domain can be determined by r_{sx} , r_{sy} and r_{sz} in *x, y* and *z* directions, and similarly, for a cubic quadrature domain, by r_{qx} , r_{qy} and r_{qz} in *x, y* and *z* directions, respectively. equations (48) and (49) show the relation of these domains with respect to local nodal spacing.

$$\begin{cases} r_{sx} = \alpha_s d_x \\ r_{sy} = \alpha_s d_y \\ r_{sz} = \alpha_s d_z \end{cases} \tag{48}$$

$$\begin{cases} r_{qx} = \alpha_q d_x \\ r_{qy} = \alpha_q d_y \\ r_{qz} = \alpha_q d_z \end{cases} \tag{49}$$

where α_s and α_q are dimensionless sizes of the support domain and quadrature domain, respectively, and d_x, d_y and d_z are the local nodal spacing in *x, y* and *z* directions. The ratio between support and local sub-domain radius can be obtained as:

$$\frac{support\ radius}{Local\ sub-domain\ radius} = \frac{r_{sx}}{r_{qx}} = \frac{r_{sy}}{r_{qy}} = \frac{r_{sz}}{r_{qz}} = \frac{\alpha_s}{\alpha_q} \tag{50}$$

The deflection is normalized by using the exact analytic solution from reference [39]. The convergence to the exact solution with the increase of the node numbers is achieved for the ratio of support radius to the radius of local sub-domain in 3.375.

The convergence rate of the central deflection of the plate for different nodal distributions with linear and second order basis is plotted in Figure 5. In this figure, the curve representing the linear basis function shows the significant locking effect which is eliminated by using the second order basis function.

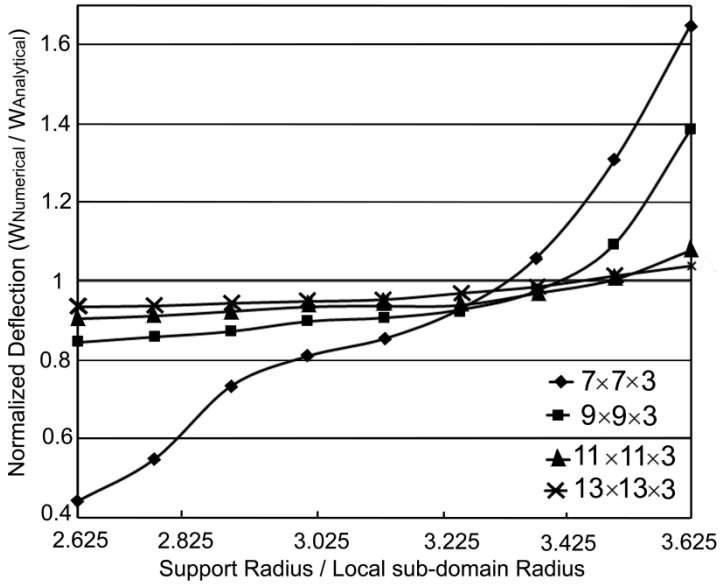

Figure 4. Normalized centeral deflection of the clamped plate for different values of ratio of the support radius to the radius of local sub-domain with different number of nodal points and quadratic basis.

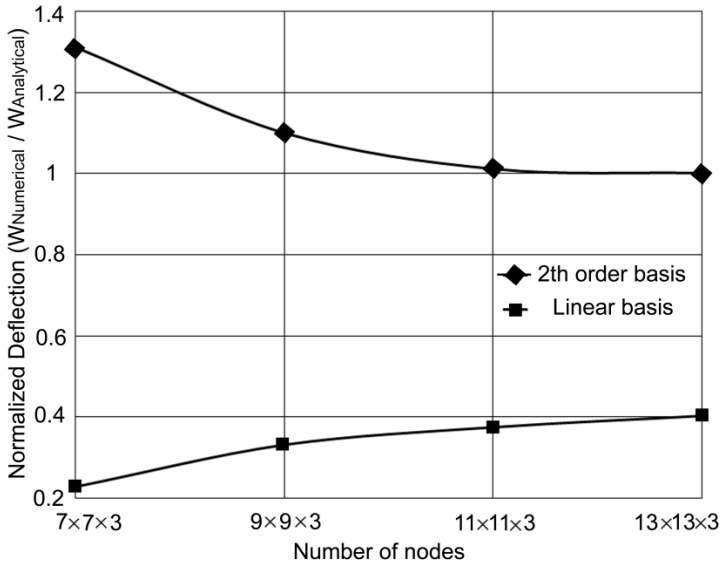

Figure 5. Convergence rate of the centeral deflection of the clamped plate.

In Figure 6 the convergence rate of the central deflection of the plate with linear basis function and different nodal points in thickness direction is plotted. As may be seen, by increasing the number of nodes in thickness direction, the convergence to the exact solution is improved, but the effect of thickness locking is not eliminated. In this regard, by comparison of Figure 5 and 6, it may be seen that by implementing second order basis function without the need of increasing the nodal points in thickness direction, the effect of thickness locking can be eliminated.

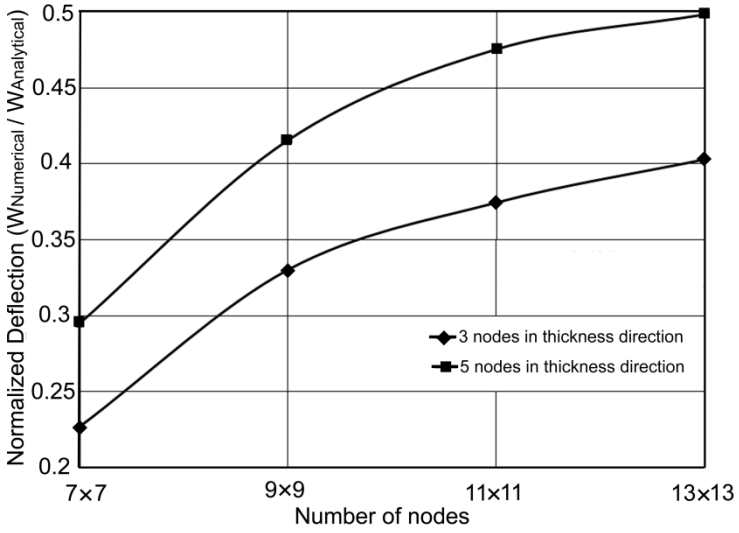

Figure 6. Convergence rate of the central deflection of the clamped plate with linear basis function.

6.2. Dynamic load

At first a clamped square plate subjected to an instantaneously applied load is analyzed (Figure 2). The amplitude of the uniformly distributed load q_0 is equal to $2.07 \times 10^6\ \mathrm{N/m^2}$. The plate thickness to span ratio is $h/a = 0.1$. For comparison, the same values of the geometrical and material parameters as used by J. Sladek et al. [31] are chosen. In particular,

the following parameters are selected: side length of the plate a = 0.254 m, thickness h = 0.0254 m, mass density $\rho = 7.166 \times 10^4$ kg/m^3, modulus of elasticity $E = 6.895$ GPa, and Poisson's ratio v = 0.3. Due to symmetry, only one quarter of the plate is discretized by the various uniformly distributed nodal points on the plate domain. The discretization by $9 \times 9 \times 3$ nodes is shown in Figure 3.

Figure 7 shows the time-variation of central deflection of the clamped square plate. The dynamic deflection is normalized by the static one, which for the considered geometry and load is w_{static} = 0.00105 m. Time is normalized by $t_0 = a^2/4\sqrt{\rho h/D} = 1.35 \times 10^{-2}$ s and $\Delta t = 1.5 \times 10^{-4}$ s used as time step.

In the second example, a clamped square plate subjected to two different loading conditions is analyzed. The geometry and nodal distributions are same the as the previous example (Figure 2 and 3). These two different loading conditions can be seen in Figure 8. The amplitude of the uniformly distributed load is $q_0 = 1000g(t)$ N/m^2. The plate thickness to span ratio is h/a = 0.1. In this example, the following material constants are considered: Young's modulus $E = 1$ Mpa, Poisson's ratio v = 0.3 and the mass density $\rho = 1000$ kg/m^3. At first the plate is subjected to an impact load which can be seen in Figure 8a. Afterwards the time-step load is applied to the plate (Figure 8b). In the first loading conditions $t_0 = 0$ s, $\Delta t = 0.01$ s and for the next $t_0 = 0.125$ s, $\Delta t = 0.02$ s are considered.

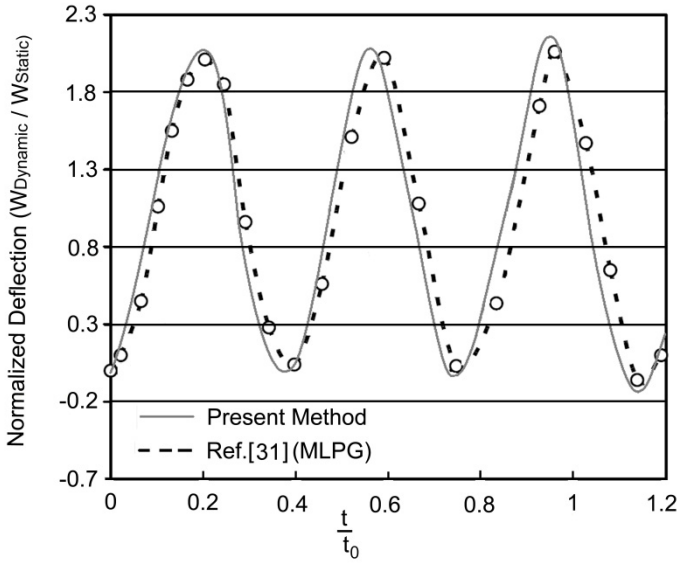

Figure 7. Time-variation of central deflection of the clamped square plate.

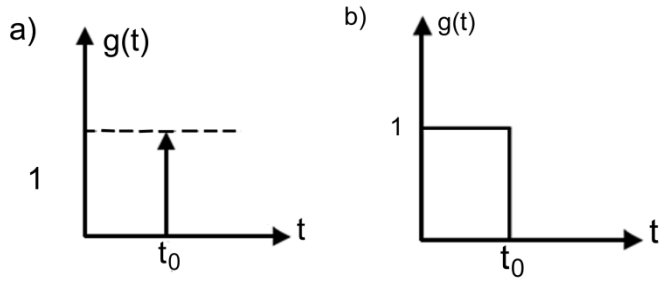

Figure 8. Applied load in two different loading conditions; a) Impact load, b) Time-step load.

Figure 9, shows time-variation of central deflection of the clamped square plate under impact and time-step loads. Here again, dynamic deflection is normalized by the static value.

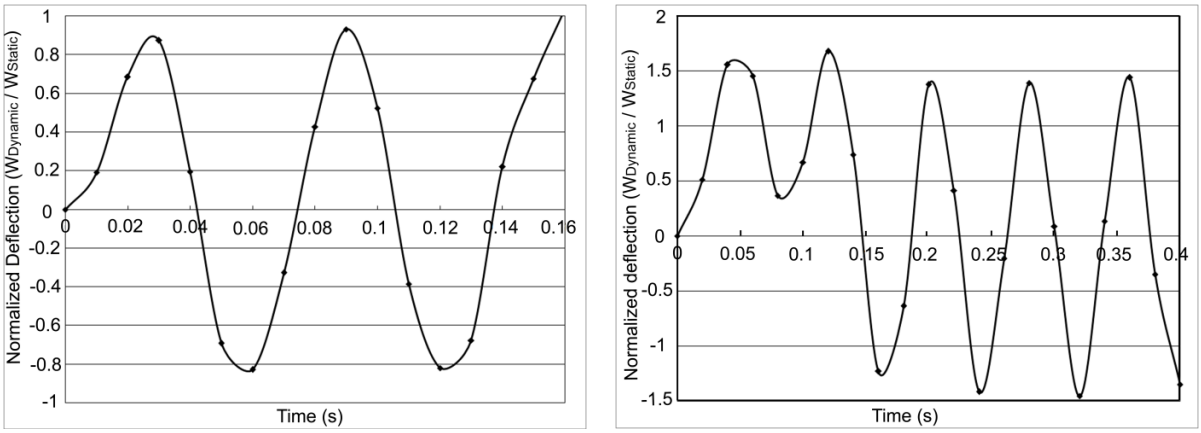

(a) (b)

Figure 9. Time-variation of central deflection of the clamped square plate. a) Impact load, b) Time-step load.

In the impact loading condition, a steady harmonic vibration should be observed around the zero. In the time-step loading, until t_0 dynamic deflection of the plate fluctuate around the static deformation given by static analysis and after this around the zero, according to the equilibrium position.

In the last example, a square cantilever plate subjected to a shear load along the free end is analyzed (Figure 10). The material constants are considered as follows: Young's modulus $E = 69$ Gpa, Poisson's ratio v = 0.33 and the mass density $\rho = 2900$ Kg/m^3. The shear wave velocity for the considered material is c_2 = 2990 m/s and $\Delta t = 2 \times 10^{-4}$ s is used as time step. The following geometrical parameters are used in our numerical calculations: the side length of the plate a = 0.2 m and the thickness h =0.02 m. The same plate problem was analysed by J. Sladek et al. [31].The time-variations of the plate deflections at the end of the plate are presented in Figure 11. Here again, the numerical results are normalized by their static value w_{static} = 1.08 × 10^{-9} m corresponding to a shear loading q_0 = 1 N/m^2. The plate geometry is discretized by $13 \times 3 \times 3$ nodes.

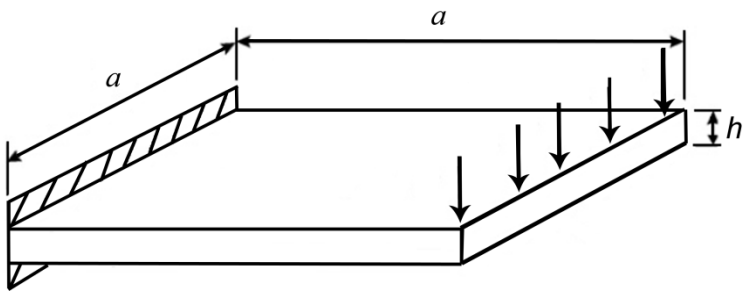

Figure 10. A cantilever square plate subjected to shear load along the free end.

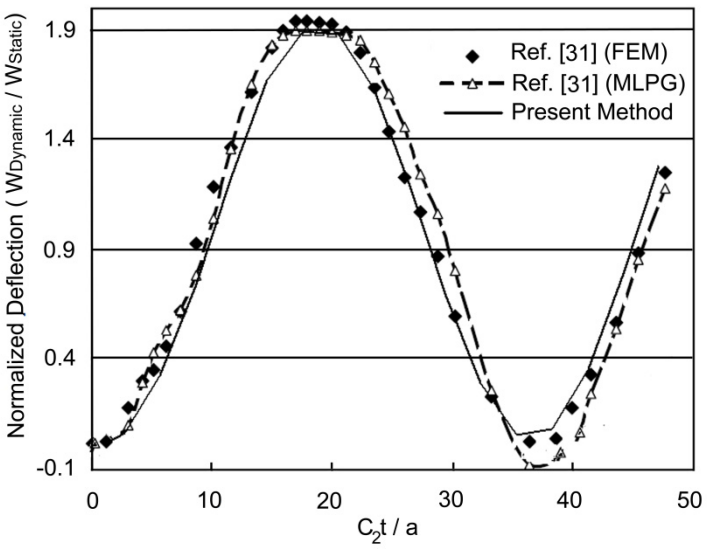

Figure 11. Time-variation of central deflection of the cantilever square plate subjected to a suddenly applied shear load.

It can be seen that the results obtained by the present method are in good agreement with those obtained by J. Sladek et al. [31].

7. Conclusion

In the present paper, Meshless Local Petrov-Galerkin method is developed for three dimensional static and dynamic analyses of thick plates. This numerical method is truly meshless because no elements or background cells are involved in either interpolation or integration. Local weak form of equilibrium equation is derived based on kinematics of a three dimensional continuum. Nodal points are distributed in the 3D analysis domain to discrete the geometry of plate. Three dimensional Moving Least Square (MLS) approximation is used as shape function to approximate the field variable of scattered nodes in the problem domain. Linear and quadratic basis functions are implemented in MLS formulation. It is shown that by using the quadratic basis, the effect of thickness locking is eliminated. The Newmark time integration method is used to solve the system of coupled second order ODEs. The essential boundary conditions are enforced by the direct interpolation method. As results, the influence of the size of the weight function support on the plate central deflection is investigated and the convergence rate of the central deflection of the plate for different nodal distributions is introduced. Numerical examples for solving the static and transient response of the elastic thick plates are demonstrated. The numerical efficiency of the proposed meshless method is illustrated by comparing the results obtained with the reference results . These comparisons have shown that this meshless method is very effective in producing good results.

References

[1] T. Belytschko, Y.Y. Lu, L. Gu, Element-Free Galerkin Methods, *International Journal for Numerical Methods in Engineering*, 37 (1994) 229–256.

[2] W.K. Liu, S. Jun, Y. Zhang, Reproducing Kernel Particle Methods, *International Journal for Numerical Methods in Fluids*, 20 (1995) 1081–1106.

[3] C.A. Duarte, J.T. Oden, An h–p Adaptive Method Using Clouds, *Computer Methods in Applied Mechanics and Engineering*, 139 (1996) 237–262.

[4] I. Babuska, J. Melenk, The Partition of Unity Method, *International Journal **for** Numerical Methods **in** Engineering*, 40 (1997) 727–758.

[5] H. Wendland, Piecewise Polynomial Positive Definite and Compactly Supported Radial Basis Functions of Minimal Degree, *Advanced Computational Methods*, 4 (1995) 389–96.

[6] B. Nayroles, G. Touzot, P. Villon, Generalizing the Finite Element Method, Diffuse Approximation and Diffuse Elements, *Computational Mechanics* 10, (1992) 307–18.

[7] N. Sukumar, B. Moran, T. Belytschko, The Natural Element Method in Solid Mechanics, *International Journal for Numerical Methods in Engineering*, 43 (1998) 839–87.

[8] L.B. Lucy, A Numerical Approach to the Testing of the Fission Hypothesis, *Astronomy Journal*, 82 (1977) 1013–24.

[9] G.E. Fasshauer, Solving Partial Differential Equations by Collocation with Radial Basis Functions, *Proceedings of the 3rd International Conference on Curves and Surfaces*, *Surface Fitting and Multiresolution Methods*, (1997).

[10] G.M. Zhang, R.C. Batra, Modified Smoothed Particle Hydrodynamics Method and its Application to Transient Problems, *Computational Mechanics*, 34 (2004) 137- 46.

[11] S.N. Atluri, T. Zhu, A New Meshless Local Petrov–Galerkin (MLPG) Approach in Computational Mechanics, *Computational Mechanics*, 22 (1998) 117–127.

[12] S.N. Atluri, H.G. Kim, J.Y. Cho, A Critical Assessment of the Truly Meshless Local Petrov–Galerkin (MLPG), and Local Boundary Integral Equation (LBIE) Methods, *Computational Mechanics*, 24 (1999) 348–372.

[13] S.N. Atluri, T. Zhu, The Meshless Local Petrov–Galerkin (MLPG) Approach for Solving Problems in Elasto-Statics, *Computational Mechanics*, 25 (2000) 169–179.

[14] S.N. Atluri, S. Shen, *The Meshless Local Petrov–Galerkin (MLPG) Method*, Tech Science Press, 2002.

[15] S.N. Atluri, T. Zhu, The Meshless Local Petrov–Galerkin (MLPG) Approach for Solving Problems in Elasto-Statics, *Computational Mechanics*, 25 (2000) 169–179.

[16] R.C. Batra, H.K. Ching, Analysis of Elasto Dynamic Deformation Near a Crack/ Notch Tip by the Meshless Local Petrov–Galerkin (MLPG) Method, *Computer Modeling in Engineering & Sciences*, 3 (2002) 717–730.

[17] H. Lin, S.N. Atluri, The Meshless Local Petrov–Galerkin (MLPG) Method for Solving Incompressible Navier–Stokes Equations, *Computer Modeling in Engineering & Sciences*, 2 (2001) 117–142.

[18] H. Lin, S.N. Atluri, Meshless Local Petrov–Galerkin (MLPG) Method for Convection-Diffusion Problems, *Computer Modeling in Engineering & Sciences,* 1 (2000) 45–60.

[19] J. Sladek, V. Sladek, S.N. Atluri, A Pure Contour Formulation for the Meshless Local Boundary Intergral Equation Method in Thermoelasticity, *Computer Modeling in Engineering & Sciences*, 2 (2001) 423–433.

[20] S.N. Atluri, J.Y. Cho, H.G. Kim, Analysis of Thin Beams Using the Meshless Local Petrov–Galerkin Method with Generalized Moving Least Squares Interpolations, *Computational Mechanics* 24 (1999) 334–47.

[21] Y.T. Gu, G.R. Liu, A Meshless Local Petrov–Galerkin (MLPG) Formulation for Static and Free Vibration Analyses of Thin Plates, *Computer Modeling in Engineering & Sciences*, 2 (2001) 463–76.

[22] H.G. Kim, S.N. Atluri, Arbitrary Placement of Secondary Nodes and Error Control in the Meshless Local Petrov–Galerkin (MLPG) Method, *Computer Modeling in Engineering & Sciences,* 2 (2000) 11–32.

[23] H.K. Ching, R.C. Batra, Determination of Crack Tip Fields in Linear Elastostatics by the Meshless Local Petrov–Galerkin (MLPG) Method, *Computer Modeling in Engineering & Sciences*, 3 (2001) 273–290.

[24] Z. Tang, S. Shen, S.N. Atluri, Analysis of Materials with Strain-Gradient Effects: A Meshless Local Petrov–Galerkin (MLPG) Approach with Nodal Displacements Only, *Computer Modeling in Engineering & Sciences*, 4 (2003) 177–96.

[25] Y.T. Gu, G.R. Liu, A Meshless Local Petrov–Galerkin (MLPG) Formulation for Static and Free Vibration Analyses of Thin Plates, *Computer Modeling in Engineering & Sciences,* 2 (2001) 463–76.

[26] S. Long, S.N. Atluri, A Meshless Local Petrov–Galerkin (MLPG) Method for Solving the Bending Problem of a Thin Plate, *Computer Modeling in Engineering & Sciences,* 3 (2002) 53–64.

[27] L.F. Qianl, R.C. Batra, L.M. Chen, Elastostatic Deformations of a Thick Plate by Using a Higher-Order Shear and Normal Deformable Plate Theory and Two Meshless Local Petrov-Galerkin (MLPG) Methods, *Computer Modeling in Engineering & Sciences,* 4 (2003) 161-175.

[28] J. Soric, Q. Li, T. Jarak, S.N. Atluri, Meshless Local Petrov-Galerkin (MLPG) Formulation for Analysis of Thick Plates, *Computer Modeling in Engineering & Sciences*, 6 (2004) 349-357.

[29] Q. Li, J. Soric, T. Jarak, S.N. Atluri, A Locking-Free Meshless Local Petrov–Galerkin Formulation for Thick and Thin Plates, *Journal of Computational Physics*, 208 (2005) 116–133.

[30] J.R. Xiao, R.C. Batra, D.F. Gilhooley, J.W. Gillespie, M.A. Mc Carthy, Analysis of Thick Plates by Using a Higher-Order Shear and Normal Deformable Plate Theory and MLPG Method with Radial Basis Functions, *Computer Methods in Applied Mechanics and Engineering*, 196 (2007) 979–987.

[31] J. Sladek, V. Sladek, J. Krivacek, P.H. Wen, Ch. Zhang, Meshless Local Petrov–Galerkin (MLPG) Method for Reissner–Mindlin Plates Under Dynamic Load, *Computer Methods in Applied Mechanics and Engineering*, 196 (2007) 2681–2691.

[32] Q. Li, S. Shen, Z.D. Han, S.N. Atluri, Application of Meshless Local Petrov-Galerkin (MLPG) to Problems with Singularities and Material Discontinuities in 3-D Elasticity, *Computer Modeling in Engineering & Sciences,* 4 (2003) 567-581.

[33] Z.D. Han, S.N. Atluri, Meshless Local Petrov-Galerkin (MLPG) Approaches for Solving 3D Problems in Elasto-Statics, *Computer Modeling in Engineering & Sciences*, 6 (2004) 168-188.

[34] Z.D. Han, S.N. Atluri, A Meshless Local Petrov-Galerkin (MLPG) Approach for 3-Dimensional Elasto-Dynamics, *Computers Materials & Continua*, 1 (2004) 129-140.

[35] Z.D. Han, S.N. Atluri, Truly Meshless Local Petrov-Galerkin (MLPG) Solutions of Traction & Displacement BIEs, *Computer Modeling in Engineering & Sciences*, 4 (2003) 665-678.

[36] S.N. Atluri, S. Shen, The Meshless Local Petrov-Galerkin (MLPG) Method: A Simple & Less Costly Alternative to the Finite Element and Boundary Element Methods, *Computer Modeling in Engineering & Sciences*, 3 (2002) 11-52.

[37] N.M. Newmark, A Method of Computation for Structural Dynamics, *Journal of the Engineering Mechanics Division ASCE*, 85 (1959) 67-94.

[38] G.R. Liu, Y.T. Gu, *An Introduction to Meshfree Methods and Their Programming*, Springer, Dordrecht, Netherlands, 2005.

[39] S. Srinivas, A.K. Rao, Flexure of Thick Rectangular Plates, *Journal of Applied Mechanics ASME*, 40 (1973) 298-299.